ELSEVIER

Journal of Neuroscience Methods 144 (2005) 79–89

JOURNAL OF NEUROSCIENCE METHODS

www.elsevier.com/locate/jneumeth

A reusable microfluidic plate with alternate-choice architecture for assessing growth preference in tissue culture

John H. Wittig Jr.[a,*], Allen F. Ryan[b], Peter M. Asbeck[a]

[a] *Department of Electrical and Computer Engineering, 9500 Gilman Drive, Mail Code 0407, University of California, San Diego, La Jolla, CA 92093-0407, USA*

[b] *Departments of Surgery/Otolaryngology and Neurosciences, UCSD School of Medicine, 9500 Gilman Ave 0666, La Jolla, CA 92093, USA*

Received 23 June 2004; received in revised form 15 October 2004; accepted 15 October 2004

Abstract

We present the design of a chamber to evaluate in vitro how species and concentrations of soluble molecules control features of cell growth—potentially including cell proliferation, cell motility, process extension, and process termination. We have created a reusable cell culture plate that integrates a microfluidic media delivery network with standard cell culture environment. The microfluidic network delivers a stream of cell culture media with a step-like concentration gradient down a 50–100 μm wide microchannel called the presentation region. Migrating cells or growing cell processes freely choose between the two distinct chemical environments in the presentation region, but they are forced to exclusively choose either one environment or the other when they grow past a physical barrier acting as a decision point. Our fabrication technique requires little specialized equipment, and can be carried out in approximately 4 days per plate. We demonstrate the effectiveness of our plates as neurites from spiral ganglion explants preferentially grow in media containing neurotrophin-3 (NT-3) as opposed to media without NT-3. Our design could be used without modification to study dissociated cell responses to soluble growth cues, and for behavioral screening of small motile organisms.

Keywords: Microfluidics; Tissue culture; Spiral ganglion; Concentration gradient; PDMS; Neurotrophin; Neurite targeting; Alternate choice

1. Introduction

Diverse biological functions rely on the ability of cells to sense spatial variations of soluble molecules and position themselves accordingly. Such spatial variations range from abrupt transitions that seem step-like in the dimension of the sensing cells, to subtle and smooth gradients that extend over long distances. In particular, phagocytosis in the immune system is mobilized by sensing abrupt differences in the body's chemical environment at the surface of a foreign invader, while chemotaxis of paramecium may lead them away from a distant source of toxin. Many of the processes that occur during developmental differentiation appear to depend on sensing gradients: retinoic acid for anterior–posterior axis specification in the brain (Durston et al., 1989), an array of factors for tonotopic specification in the developing cochlea (Kelley and Bianchi, 2001), and neurotrophins for generalized synaptic targeting (Hall, 1992; Hopker et al., 1999). In the latter case, understanding how soluble molecules affect neural process growth has several obvious clinical implications, as central, sensory and motor nerve fibers may be severed or damaged resulting in loss of function. Regeneration of such damaged fibers requires the controlled guidance of outgrowing neurites to their respective targets, which may be either biological or prosthetic.

The movement of an organism, a cell, or a cellular process may indicate its preference for a particular envi-

* Corresponding author. Present address: University of Pennsylvania Department of Bioengineering, 3320 Smith Walk/305 Hayden Hall, Philadelphia, PA 19104-6392, USA. Tel.: +1 215 205 9103; fax: +1 215 573 2071.
E-mail address: jwittig@seas.upenn.edu (J.H. Wittig Jr.).

0165-0270/$ – see front matter © 2004 Elsevier B.V. All rights reserved.
doi:10.1016/j.jneumeth.2004.10.010

ronment. But when does a cell or cellular process decide that its current environment is ideal, and that it should cease movement? Is there a saturation point in the ability of cells to detect gradients, such that a high absolute concentration level obscures the surrounding differences in concentration? What choices do cells make when faced with competing cues? Preference can be assessed quantitatively using alternate-choice paradigms. Free-choice experiments allow the subject to shift between alternate choices during the trial, while forced-choice experiments eliminate the possibility of shifting after the initial choice is made. These alternate-choice experimental techniques can be complimentary (Ono, 2000), though the forced-choice paradigm is often preferred because it reduces experimental noise from indecisive subjects. By creating an environment where cells and organisms are presented with alternate choices between two or more experimental conditions, one may probe the ideal milieu of soluble molecules to control growth or proliferation in any background environment.

Here we describe the fabrication of a microfluidic device that allows both free- and forced-choice experiments to be performed simultaneously. Microfabrication techniques are useful for making microfluidic devices for various research applications. Methods for the rapid prototyping of microfluidic systems using a positive relief microchannel structure on silicon molded with polydimethylsiloxane (PDMS) were outline by Duffy et al. (1998). This technique formed the basis for a network used to create complex concentration gradients (Dertinger et al., 2001) with laminar fluid flow through microchannels. Microfluidic systems have been used to segregate cells for short durations (Takayama et al., 1999) and to pattern substrate-bound gradients later used to direct axon growth (Dertinger et al., 2002). This paper presents the fusion of a standard neuronal culture environment with a simple microchannel network that presents neurons with an abrupt transition in the local chemical environment for extended periods of time, thereby providing a platform for assessing growth preference using alternate-choice paradigms.

The relatively simple fabrication procedure may be performed with minimal or no use of a clean room; fabrication requires the use of a mask aligner (ultra violet lamp coupled to a microscope and movable stage), photoresist spinner, and digital hot plate. Previous microfluidic designs permanently bond fluidic delivery tubes, microchannel layers, and surface layers such that each unit can be used only once (Duffy et al., 1998; Dertinger et al., 2001). We use a compression plate to make each unit reusable across experiments. The compression plate incorporates a fluidic delivery system, simplifying connection of a hydraulic pump (syringe pump) to the cell culture plate. Tissue culture experiments were performed using explants of neonatal spiral ganglion neurons from the rat cochlea and neurotrophin-3 (NT-3), since the responses of these neurons to this factor have been extensively characterized (Aletsee et al., 2001a, b, 2002; Hossain et al., 2002).

2. Materials and methods

2.1. Design constraints

We have designed integrated microfluidic (IMF) tissue culture plates that integrate a microfluidic media delivery network with a standard tissue culture environment. We required that the IMF plates be incorporated into our existing neural tissue culture setup to minimize laboratory reorganization and to provide direct comparison with our other spiral ganglion culture results (e.g. Aletsee et al., 2001a, b, 2002; Brors et al., 2003). Our plate design utilizes three spatial scales; a micro (50–100 μm) channel dimension to assess neurite preference, a macro (1 cm^3) tissue well dimension to promote efficient gas exchange and tissue loading, and an intermediate (0.5–1 mm) tissue containment dimension to minimize tissue damage during positioning of the spiral ganglion explant at the microchannel opening. Due to the use of multiple spatial scales, we are able to accurately position 300 μm × 300 μm tissue explants within 500 μm of the microchannel network mouth. This distance is close enough for extending neurites and proliferating glial cells to experience a stable and reproducible concentration gradient formed at the mouth of the microchannel network. Further design constraints included: the ability to precisely control flow rate through the microchannels, a cheap disposable surface for irreversible tissue adhesion, and an optical pathway for tissue visualization with an inverted fluorescence microscope.

Top and side views of the IMF mold and the assembled IMF tissue culture plates are schematized in Fig. 1. Our fabrication process consists of three steps (Fig. 2): microfabricating the positive relief mold master using photolithography, casting the reusable IMF mold, and assembling the compression plates. Our microfabrication process only need be carried out once per microchannel design, as the mold master is semi-permanent. We create as many reusable IMF molds and compression plates as can be supported by our tissue culture setup. The results presented here come from several week-long experiments using four to eight IMF tissue culture plates in parallel. Our process of using the IMF tissue culture plates is described in three sections below: pre-experiment preparation, IMF plate setup (Fig. 3), and integrated tissue culture. In the following sections, we detail both the fabrication and use of the IMF plates in spiral ganglion explant tissue culture.

2.2. Microfabricating the mold master

Our photolithographic process uses two aligned masks, both designed using Canvas 5.0 (Deneba Systems Inc.) and printed as high-resolution transparencies from a 1400 dpi laser printer (Linotronic 330). In Fig. 4, we demonstrate the alignment of our two-mask set, with gray defining the 50 μm thick microchannels, and white defining the 500 μm thick intermediate layer. We use positive-photoresists in our process; the resist that is exposed to light hardens and the rest

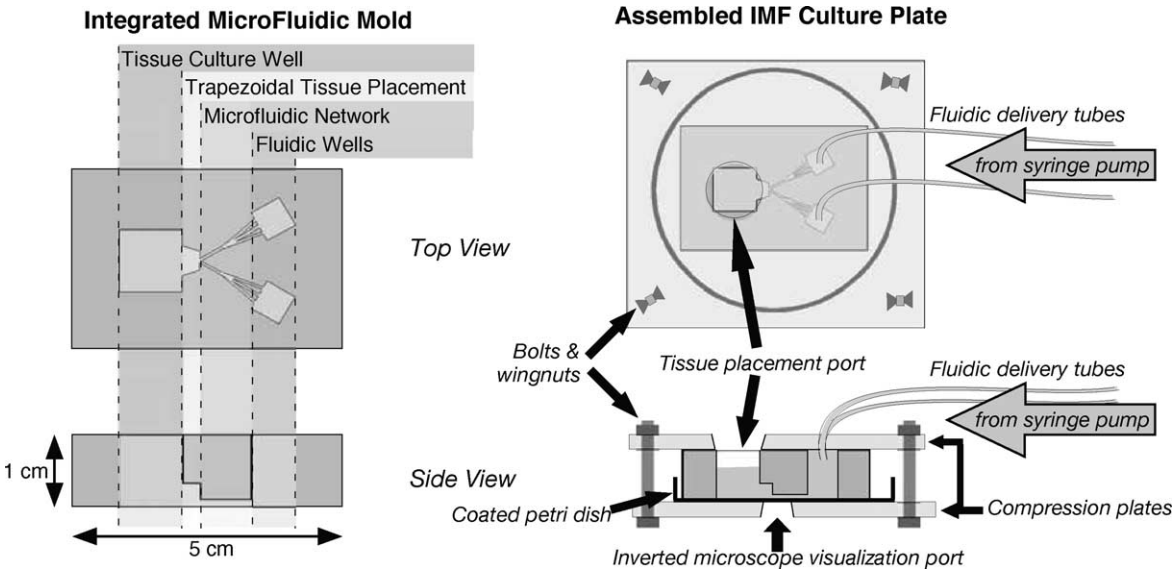

Fig. 1. Schematic view of integrated microfluidic mold and assembled IMF tissue plate. (Left) The integrated microfluidic mold is cast from the silicone elastomer PDMS. The mold dimensions are approximately 3 cm × 5 cm × 1 cm. Regions of interest within the mold are indicated above the schematic. (Right) The assembled IMF tissue culture plate. Two plexiglass plates compress an IMF mold onto a coated 60 mm petri dish. Culture media is delivered from a syringe pump through the fluidic delivery tubes into the microfluidic network.

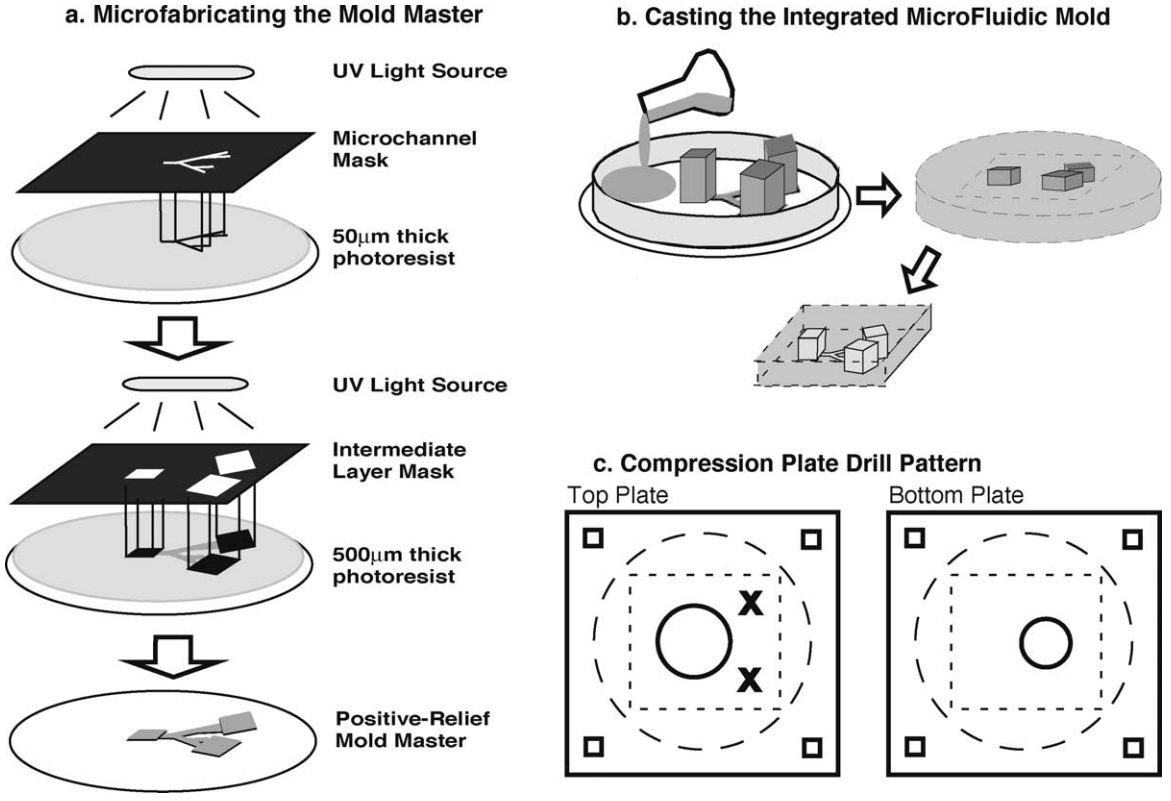

Fig. 2. Integrated microfluidic mold fabrication. (a) Photolithographic process using two mask sets and the ultra viscous photoresist SU-8. A UV light source shines through the masks to create the microchannel and intermediate layers. Arrows indicate various fabrication steps (see Table 1) including heating, photoresist application, and development. The final product is a positive relief mold master. (b) Casting the IMF mold using PDMS. Intermediate layer alignment posts are used to position and hold aluminum blocks that create macroscopic wells in the mold. Mold is cured at 75 °C for 24 h, then blocks are removed and individual units are excised. (c) Drill patterns for top and bottom compression plates. Symbols represent aligned bolt holes (squares), fluidic delivery holes (×), petri lid outline (dashed circle), IMF mold outline (dashed rectangle), and tissue placement/visualization ports (circles).

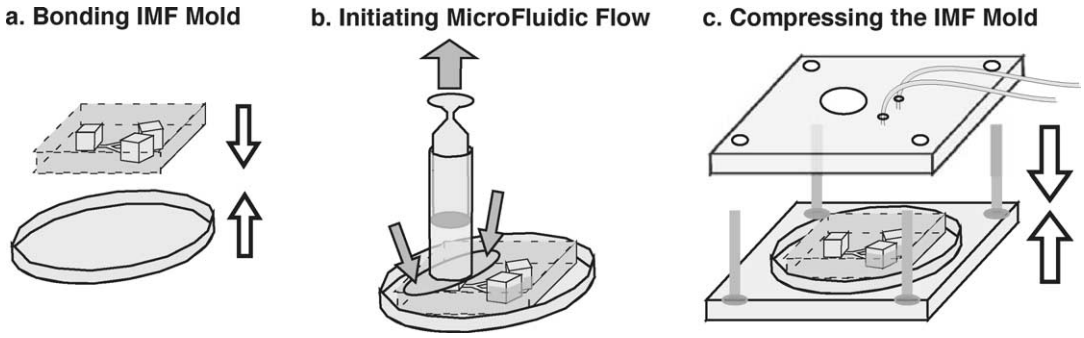

Fig. 3. Integrated microfluidic tissue culture plate setup. (a) IMF mold is reversibly bound to a treated petri dish lid. (b) Vacuum is applied to the tissue well with a cut syringe to initiate flow in the microfluidic network. (c) Compression plates are aligned around the bound IMF mold and the fluidic wells are filled as the plates are bolted together.

is washed away during development. Therefore, the schematized gray microchannels, and white intermediate regions in Fig. 4 are actually transparent on our masks. Our microchannel regions extend into the intermediate regions by more than 10 μm at each connection point to guarantee fluidic continuity in the IMF molds. The microchannels fan out as they approach the fluidic delivery wells to prevent channel blockage by small particles, and to avoid permanent mold master damage due to channels breaking during mold release. We use the intermediate (500 μm) layer to define the trapezoidal tissue placement regions as well as the rectangular aluminum block alignment posts which are used during mold casting. We optimize area in our tissue culture incubator by conducting two experiments per IMF plate, both tissues sharing a common central placement and gas exchange well, but each tissue having independent fluidic delivery inputs for precise flow rate control. Diagrams in Figs. 1–3 present a simplified schematic with a single microchannel network per tissue well.

The specifics of our microfabrication process are detailed in Table 1. We create the mold master on a clean 4 in. silicon wafer; chosen because it is perfectly flat, readily conducts heat, and minimally absorbs the solvents used during fabrication. We use the full surface of the 4 in. wafer by spacing four independent IMF mold masters (3 cm × 5 cm each) across it. We use two viscosities of ultra thick positive-photoresist for our two layers; SU-8 100 and SU-8 1000 (Microchem Corporation). After thoroughly cleaning the silicon wafer, approximately 3 ml of room temperature photoresist is evenly applied across the entire wafer surface. The wafer is then spun around its center for the allotted durations and speeds to yield a consistent photoresist thickness. A digital hot plate with a ramping function (Coleman-Palmer) is used for all heating steps in the process. The thickness of our photoresist layers requires bottom surface heating—ovens are ineffective. After pre-bake, we compress the appropriate transparency mask onto the semi-hardened photoresist and align as necessary using a microscope. The exposed regions of the microchannel

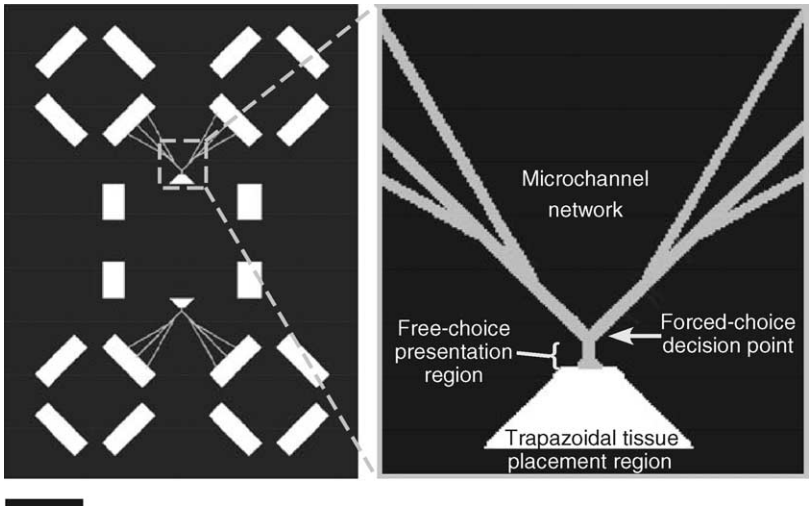

Fig. 4. Photolithographic masks for microfabrication. Overlay of two masks used to microfabricate the positive relief mold master. Gray solid regions define the 50 μm thick microchannel layer, and white regions define the 500 μm thick intermediate layer. (Left) An isolated IMF mold master is approximately 3 cm × 5 cm. Large white rectangles define the alignment posts used to hold aluminum blocks during mold casting. Two microfluidic networks feed into the central tissue culture area. Each network is fed by two fluidic wells. (Right) Magnified image of the trapezoidal positioning region (intermediate layer), the free-choice presentation region and the forced-choice decision point of the microfluidic network. Scale bar at the bottom is 4.5 mm (left) and 0.55 mm (right).

Table 1
Mold master fabrication details

Clean silicon wafer and aluminum blocks
Sonicate in acetone 10 min, methanol 10 min, and blow dry with N_2
Microchannel (50 μm) layer
Cover wafer with ∼3 ml room temperature SU-8 100 photoresist
Spin coat 50 μm layer of SU-8 100 (600 rpm for 20 s)
Pre-bake on hot plate (50–90 °C 20 min, 90 °C 20 min)
Cover with microchannel mask and expose with UV light (250 s)
Post-bake (50–90 °C 10 min, 90 °C 10 min)
Intermediate (500 μm) layer
Cover wafer with ∼3 ml room temperature SU-8 1000 photoresist
Spin coat 500 μm layer of SU-8 1000 (600 rpm for 40 s)
Pre-bake on hot plate (50–95 °C 1 h, 95 °C 1.5 h)
Align intermediate mask and expose with UV light (700 s)
Post-bake (50–90 °C 10 min, 90 °C 20 min)
Development and hardening
Develop SU-8 photoresist (15 min + 13 min + 2 min fresh developer)
Rinse isopropyl alcohol (30 s)
Carefully blow dry with N_2 in the direction of the channels
Hardening bake at 120 °C (1 h)
Evaporation at room temperature under vacuum (36 h)
Epoxy wafer onto oversized aluminum plate (3 mm thick × 13 cm × 13 cm)

layer become translucent after post-bake, therefore alignment of the second mask is possible by directly observing overlap between transparent intermediate layer regions in the second mask and translucent channel regions close to the surface of the silicon wafer. Ultra violet exposure times are based on a HGK mask aligner with a 600 W power supply, but may be adapted to a simple UV desk lamp (Vozzi et al., 2002, 2003). Development is carried out with gentle agitation in three consecutive steps in separate glass containers holding fresh developer. Care must be taken not to blow nitrogen against the direction of the microchannels, as this may lift the microchannels off the wafer. After the mold master is cleaned, hard-baked, and dried, we epoxy it to a 3 mm thick aluminum plate to prevent shattering the wafer during mold release.

2.3. Casting the IMF mold

We use the silicone elastomer polydimethylsiloxane (Sylgard 184, Dow Corning), previously used in various microfluidic applications (Duffy et al., 1998; Vozzi et al., 2002, 2003). This silicon-based molding agent faithfully resolves micron-level details and can be cured to various degrees of compressibility depending on cure temperature. We have found thorough mixing imperative for creating a reusable mold with the large dimensions we are interested in. We therefore mix the elastomer and curing agent with a power mixer for one hour, and then fully evacuate all bubbles in a desiccation container under vacuum. We place the mold master (adhered to an aluminum plate) on our hotplate with a vacuum-grease sealed plastic ring surrounding the entire wafer. We then carefully place custom cut and ethanol cleaned aluminum blocks (2 cm × 1 cm × 1 cm tissue culture well, 2 cm × 0.5 cm × 0.5 cm fluidic wells) within the aluminum block alignment posts and slowly pour the PDMS to a height of approximately 1 cm. The mold is cast at 75 °C for 24 h, followed by slow cooling to room temperature. This curing temperature stiffens the PDMS sufficiently to reduce deformation of the microchannels when compressing the IMF mold. The PDMS with aluminum blocks is carefully pealed from the mold master and is placed on a clean surface for cutting and aluminum block removal. Individual molds are examined under microscope; forceps are used to clear excess PDMS and photoresist that was lifted from the mold master.

2.4. Assembling the compression plates

Our plates are cut from 3.2 mm thick bicarbonate Plexiglas large enough to fully surround the 60 mm petri dishes used in our experiments. In Fig. 2c, we diagram drill patterns for the top and bottom compression plates. The top plate has seven drill holes; four at the corners for bolting the plates together, two allowing fluidic delivery tubing access, and one tissue placement and gas exchange port. The bottom plate has four holes for bolting the plates together, and one for visualization of the tissue with an inverted microscope. The tissue placement and gas exchange port need be large enough to allow surgical forceps access to the trapezoidal tissue-positioning region of the plate. The small fluidic delivery holes are designed to snuggly fit 20-gauge tubing, which is permanently connected to the top plate using 5-min epoxy. The other end of the tubing is attached to 20-gauge syringe needles, which are connected to three-way valves and 1 ml syringes. We load arrays of syringes into a digital syringe pump (Harvard Instruments) with a custom made honeycomb-like syringe array holder allowing us to run four parallel experiments with a single syringe pump. We use approximately 1 m of tubing between the top plate and syringe pump—long enough to extend from the IMF plates inside our incubator to the modified syringe pump placed on top.

2.5. Pre-experiment preparation

We prepare for each tissue culture experiment by cleaning reusable components, coating the disposable adhesion surface, and equilibrating the tissue culture media to our incubator's temperature and gas concentrations. We clean the IMF molds by wiping with an ethanol soaked Kimwipe, followed by 10 min sonication in ethanol and evaporative drying in a sterile tissue culture hood. The compression plates are cleaned with soap and water, and the fluid delivery tubes are flushed with ethanol. All reusable components are EtO gas sterilized to avoid heat degradation and water absorption that occurs during autoclave sterilization. We coat a sterile, disposable 60 mm petri dish with

poly-L-lysine (1 mg/ml) for 1 h at 37 °C, rinse with phosphate buffered saline (PBS), coat with Laminin (10 μg/ml) at 4 °C overnight, rinse with PBS, and evaporate dry in a tissue culture hood. Our established culture protocol consists of two stages of culture media (Aletsee et al., 2001a, b, 2002), both using Dulbeco's Modified Eagle Medium (DMEM) as a base; an adhesion media (25 mM HEPES, 300 U/ml penicillin, 10% FBS) for attachment during the first 12–18 h in culture, followed by a growth media (25 mM HEPES, 300 U/ml penicillin, 30 μl/ml N_2, 6 mg/ml glucose) with and without the diffusible molecule we are assessing, NT-3 (25 ng/ml). All media constituents are purchased from Sigma–Aldrich. We prepare all culture media solutions in open containers and incubate (pO_2 0.95, pCO_2 0.05, 37 °C) for 30 min before drawing the growth media into labeled 1 ml syringes.

2.6. IMF plate setup

Our IMF plate is setup in a series of steps (Fig. 3): bonding the IMF mold and coated petri dish, initiating flow in the microchannels, flushing the fluidic delivery tubing and wells, applying the compression plates, and adjusting compressive tension while removing air bubbles. We have found vacuum most effectively initiates fluid flow in the microchannels. In a tissue culture hood, we apply a controlled vacuum via a modified 3 cm^3 syringe; its head is cut off, and the plunger is reinserted from the opposite side to make vacuum application easier. We fill the fluidic wells with their respective media, and place the back end of the 3 mm syringe over the tissue culture well while applying suction to initiate flow and clear bubbles from the network (see Fig. 3b). Fluidic continuity is confirmed using an inverted microscope before proceeding to the next step. We then top off the fluidic wells with their respective media and flush the fluidic delivery tubes with culture media to avoid having a compressible gas pocket in the fluid path during the experiment. We align the compression plates above and below the bound IMF mold and tighten the wing nuts such that all fluid trapped between the top compression plate and the top surface of the IMF mold is displaced. We visualize the microchannels with an inverted microscope while adjusting compression plate tension to minimize deformation of the microchannel structures yet maintain a seal between the top of the IMF mold and the upper compression plate. We then use fine forceps to remove air bubbles from the trapezoidal tissue placement region. Finally we micropipette the mixed growth media from the tissue culture well and fill the well with adhesion media. The assembled tissue culture plate is then stored in the incubator to equilibrate the media temperature and gas concentration while dissections are performed.

2.7. Integrated tissue culture

After setting up our IMF plate, our existing tissue culture procedure (e.g. Brors et al., 2003) is followed with little modification. We dissect the spiral ganglion from neonatal (P3–P5) rat cochleae and cut the tissue into approximately 300 μm × 300 μm explants. With fine forceps we transfer the explants to the tissue culture well and gently push them into the trapezoidal tissue placement region as close to the microchannel opening as possible. We avoid moving the fluidic delivery tubing after the tissue has been positioned, since minute flow in the microchannels can displace the explant before it adheres to the petri dish surface. After 12–18 h we connect the closed three-way valves at the ends of the fluidic delivery tubes to the appropriate growth media filled syringes loaded into the modified syringe pump. Valves are opened, and pumping is carried out for 72 h at 15–30 μl/h. After pumping, we remove most of the media from the tissue culture well, rinse (PBS) and apply fixative (4% paraformaldehyde in PBS) to the explants before immunostaining. When removing fluid from the well we use a micropipette and always leave a meniscus to avoid dislodging the explants. Fixative is gently drawn into the microchannel structure by setting the syringe pump to withdraw at a rate of 5 μl/min for 3 min; if the fluid level in the well becomes low we immediately refill it. We allow the fixative to take action for 25 min at room temperature before proceeding.

All subsequent immunostaining steps are performed with the syringe pump set to withdraw for 3 min per step, followed by the specified incubation period for each step. Steps are carried out at room temperature unless otherwise stated. After fixing we wash twice with PBS. We then lyse with 1% Triton in PBS for 10 min, and wash once with PBS. Nonspecific binding is reduced by incubating with 1% donkey serum (Sigma–Aldrich) for 25 min. In order to detect 200-kDa neurofilaments, the explants are incubated at 4 °C overnight with a polyclonal anti-neurofilament antibody (Sigma–Aldrich) developed in rabbit and diluted 1:500 in 1% donkey serum. The explants are then incubated for 2.5 h at room temperature with fluorescein isothiocyanta (FITC)-conjugated donkey anti-rabbit secondary antibody (Jackson ImmunoResearch) diluted 1:100 in 1% donkey serum, followed by a final wash with PBS. We visualize and store images of the stained processes using an inverted fluorescent microscope with a digital camera and frame grabbing software (Spot camera and software, Diagnostic Instruments Inc.). We then disassemble the specialized plate, disposing of the used petri dish, and clean the various components as described above.

3. Results

3.1. Fluid distribution in the microchannels

We assess growth preference using a simple microfluidic network to present extending neurites with a step-like gradient within the presentation region, thereby creating two distinct environments to choose between. Within the free-choice

presentation region growing specimens are able to choose either or both environments. The presentation region further acts to guide growing specimen toward the forced-choice decision point, which is defined by the split in the microchannel "Y" (Fig. 4). The microchannels that come together to form the forced-choice decision point provide the flow which sets up the free-choice gradient, thereby allowing the simultaneous use of both paradigms. Gradient sharpness is controlled by the flow rate in the microchannels, while gradient endpoints are specified by the media compositions used in the device.

We have tested gradient formation in our microfluidic network using the florescent molecule Biodipy green (Molecular Probes). The gradient we analyze in Fig. 5 was formed after flowing media for 20 min at a rate of 33 μl/h. As can be seen from the figure, from the top to the widest segments of the presentation region fluid mixing and diffusion is minimal, resulting in a sharp gradient between the two fluids along the length of the microchannel. Once the fluids exit the microchannel into the trapezoidal tissue placement region, concentration decreases as the volume increases and mixing occurs. The tissue placement region thus provides a broad gradient of concentrations, while the entire presentation region provides an area of well defined free-choice between two media leading up to the forced-choice decision point.

To assess this fluid behavior quantitatively, we measure image intensity across the channel width at three locations in the microchannel network and fit using the theoretical solution to a step gradient that relaxes with time (Weiss, 1996):

$$\text{Concentration}\,(x, t_{\text{relax}}) = C_{\text{Low}} + C_{\text{Diff}} \times \int_{-\infty}^{x/\sqrt{2Dt_{\text{relax}}}} \frac{1}{\sqrt{2\pi}} e^{-y^2/2} \mathrm{d}y$$

where x represents the distance in microns from the center of the microchannel width, t_{relax} the amount of time the step gradient is allowed to relax, C_{Low} the lower concentration value, C_{Diff} the difference between the two test concentrations, and D is the diffusion coefficient of the molecule under consideration. We adjusted the digital integration of our camera to avoid saturation where we measured image intensity across the channel width; therefore we assume intensity varies linearly with concentration when fitting with this equation. We estimate Biodipy's diffusion coefficient to be 10 $\mu m^2/s$ (Gribbon and Hardingham, 1998), and fit each set of experimental points by varying the relaxation time, t_{relax}. This value describes how long it would take an initial step-like gradient of Biodipy to diffuse to the observed concentration gradient. The best fit relaxation times at the top, middle, and widest part of the presentation region are 3.5, 7.5, and 32 s, respectively. The non-zero top relaxation time indicates that this gradient is not a perfect step, and therefore mixing occurs as the two media channels come together. We expect a relaxation time difference of 55 ms if laminar flow carries media from the top to the middle of the microchannel. The observed difference in relaxation time of 4 s suggests lateral mixing continues during flow in the laminar region. The final relaxation time of 32 s is not directly comparable to the other measurements, as the channel width increases significantly. We use this increase in width to maximize the preference assessment area for growing specimens that terminate upon entering the free-choice region. We show the 10 and 90% concentration lines on the plots in Fig. 5; the choice of specimens that terminate between these lines is considered ambiguous in terms of environmental preference. The ratio of preference assessment area and total channel width in microns is 68–100 and 184–250 at the middle and widest part of the channel, respectively.

We assume the two test media mix as they flow from the microchannel network into the trapezoidal tissue placement region due to the dramatic increase in vertical and horizontal dimension (10 times the height and three times the width). We expect this mixing to result in a smoothed gradient emanating from the channel mouth, as predicted by mixing observed in other microfluidic systems (Weigl et al., 2001), and as evidenced by distant neurite attraction to the channel mouth (observed in Fig. 6a). Approaching neurites will therefore experience mixture of the two media sources while approaching the microchannel mouth from the tissue placement region. We could not accurately measure the gradient in this region, perhaps because the increased depth of field in the 500 μm thick region led to saturation of our imaging system.

3.2. Cell culture assays

We test the performance of the microfluidic plate by assaying the preference of spiral ganglion neurons for NT-3. Control explants are presented growth media with equal concentrations (25 ng/ml) of NT-3 in both of the fluidic delivery channels. Alternate-choice preparations are presented media with 25 ng/ml NT-3 in one fluidic delivery channel (+) and media with no NT-3 in the other channel (−). We have imaged seven alternate-choice and three control explants in the IMF culture plates, 40% of which extended their processes into the presentation region for analysis. Fig. 6a and b shows two explants with neurites extending into the microchannel network during alternate-choice experiments. Neurites are observed making a sharp change in direction in Fig. 6a, which may have occurred at the onset of microchannel flow after 18 h of adhesive growth, based on neurite length before and after the turn. The frequency of neurite extension into the microchannel network and salient changes in neurite growth direction during some experiments provides qualitative evidence that spiral ganglion explants grow towards a media rich in NT-3.

We quantify alternate-choice decisions as the number of neurite terminals observed within the preference assessment areas of the presentation region. The diffusion coefficient of NT-3 is lower than that of our florescent test molecule (Negro et al., 1994; Weiss, 1996; Chang and Popov, 1999), so we

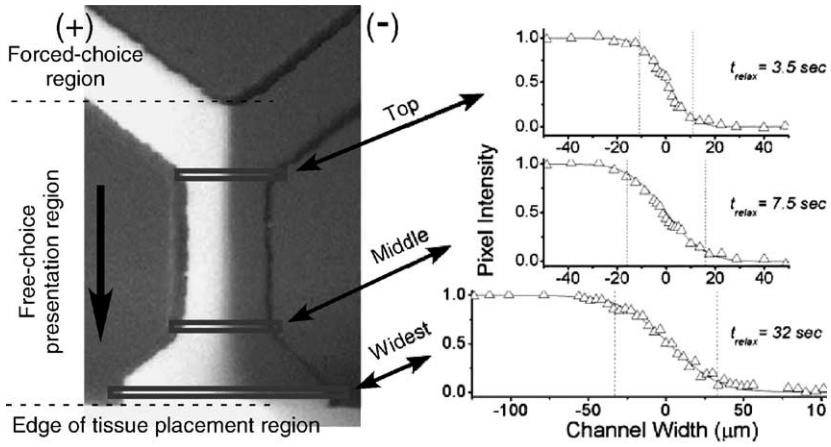

Fig. 5. Gradient formation assessment. (Left) Digital image of florescent in the microchannel network resulting from 20 min pumping media solutions at 33 μl/h with (+) and without (−) the florescent indicator Biodipy green. Media flows from the top of the image downward. (Right) Normalized pixel intensity values (triangles) across the channel width for three regions of the microchannel; top, middle, and widest. Abscissas indicate position across the microchannel width in microns, with the center of the channel equal to zero. Intensity data are fit with the theoretical solution to step gradients (blue line, equation in text) with the best fitting relaxation time given in seconds on the right. We define preference assessment area as the region where concentration is above 10% and below 90%; these intensity values from the theoretical fit are denoted with vertical dashed lines in the plot. The abscissa scale of the 'widest' plot is condensed relative to the other two graphs to show the theoretical fit across the entire channel width.

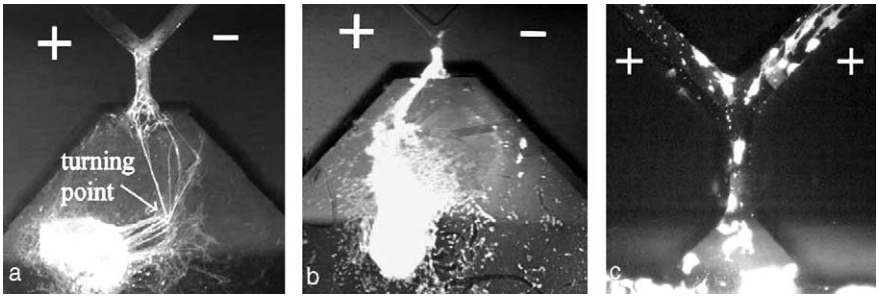

Fig. 6. Tissue culture results. Three imaged explants. In all images (+) and (−) indicate which delivery channel carried the neurotrophin NT-3 (+) and which did not (−). All cultures are labeled with polyclonal anti-neurofilament primary and FITC-conjugated secondary antibodies. (a) Individual neurites can be discerned entering, branching, and terminating within the free-choice region of the microchannel network. (b) A fiber bundle consisting of many neurites terminating within the free-choice region. (c) Glial cells growing past the forced-choice decision point in a control (NT-3/NT-3) experiment.

are actually underestimating the preference assessment area in our analysis. Neural growth cones extend filopodia tens of microns to sample the immediate vicinity of the growth cone (Murray and Whitington, 1999). Therefore, within the 50–100 μm wide presentation region they can sample both chemical environments being tested. Since neurites tend to collapse and withdraw filopodia that encounter unfavorable conditions, and grow in the direction of filopodia that encounter favorable conditions, one would predict that neurites would tend to terminate on the NT-3 containing side of the channel. This is indeed what we see in 71% of the observed neurites (Table 2). Our staining method equally labels the axons and dendrites of the normally bipolar spiral ganglion neurons, and as such we cannot make conclusions about what type of neurite exhibits the observed NT-3 preference.

In four experiments, we observed glial cell growth into the microchannel network (Fig. 6c). Glial cells are present in our spiral ganglion explants and they typically grow out

Table 2
IMF tissue culture results

	Control: flow 100%/100% NT-3	Experiment: flow 100%/0% NT-3
Total explants imaged	3	7
Explants with neuritis	3	6
Explants with neurite growth into free-choice region of the microchannel network	1	3
Neurites terminating in 25 ng/ml NT-3	1	5
Neurites terminating in 0 ng/ml NT-3	Not applicable	1
Neurite terminating in ambiguous center region	Not applicable	1
Percent neurites showing free-choice preference for 25 ng/ml NT-3	–	71%

from the explant in all directions. We use a polyclonal anti-neurofilament antibody that labels glial and spiral ganglion cell bodies sufficiently for visualization. We observed glial cell proliferation throughout the microchannel network in three control experiments (as shown in Fig. 6c), and only in the NT-3 rich microchannel during a single preference assessment experiment (data not shown). Therefore, we make no conclusions regarding glial cell growth preference, though glial cell growth past the forced-choice decision point demonstrates the versatility of the IMF tissue culture plate for assessing cell growth and proliferation.

4. Discussion

We have created an IMF tissue culture plate to compare the effects of different species and concentrations of soluble molecules on cell growth—including proliferation, motility, process extension, and process termination. Our results demonstrate that the fluid delivery and cell culture components function and are compatible at the flow rates tested. Following the alternate-choice paradigm, we quantitatively assess preference by subjecting growing cells to a step-like gradient of soluble environmental conditions. Within the microchannel presentation region, extending processes or migrating cells are free to choose either or both conditions. At the branch point of the "Y", individual neurites or cells are forced to choose between one condition and the other. Preference can be evaluated both within the presentation region and by choices made at the branch point. We used a florescent indicator to confirm gradient sharpness throughout the microchannel presentation area. The more gradual and increasing gradient in the trapezoidal tissue placement region allows neurites and cells to select from a broader range of concentrations, and to follow an increasing gradient toward the microchannel network. Our results indicate that both neurites and glial cells will grow into the microchannel network. The IMF tissue culture plate is reusable, and therefore our four-day fabrication process is iterated only to increase the number of plates available for parallel experiments.

Neurites and glial cells appear to prefer NT-3 when given a choice between media with the factor and media without the factor. This finding cannot be predicted from the results of our standard in vitro assays in which we compare the number of neurites extending from spiral ganglion explants in media with or without NT-3 (e.g. Aletsee et al., 2001a, b). The results from our IMF plates may be compared to other site-directed presentations of growth signals. Early in vitro work establishing developmental effects of neurotrophins (Campenot, 1982) relied on media separation using petroleum jelly, which lacks the spatial scales and reproducibility possible using microfabrication. More recently, use of a semi-permeable membrane demonstrated that neurites proliferate more in media containing NT-3 (Malgrange et al., 1996a, b), though this assay did not provide a directional signal. Delivery of NT-3 from a micropipette can induce directional responses from growing neurites (Song et al., 1997), but result in a gradient that is difficult to quantify. Another technique presents a localized growth factor covalently bonded to microspheres (Aletsee et al., 2003). Although this method allows for co-varying bath and microsphere environments, local gradients setup by growth factors diffusing from the spheres are hard to define, and physical cues resulting from the microspheres themselves may obscure results. Similarly, co-culture of neurons with transfected cells expressing growth factors (e.g. Dazert et al., 1998) fails to provide defined gradients and may introduce confounding variables due to physical cues from the secreting cells, although this technique provides insight into neurite targeting in an arguably more physiological setting. In contrast, the gradients setup within the presentation region of the IMF plate are well-characterized and stable, and within the presentation region there is no physical boundary between the two environments presented. The precise control of test concentrations in the IMF device provides the ability to compare responses to two defined conditions. Combined with the ease-of-use and versatility of the plate, this makes the IMF device a valuable tool for rapidly determining tropic factor preferences under various background conditions.

Our present results demonstrate the IMF device can be used to study NT-3 mediated growth preference in spiral ganglion and glial cells; additional experiments using the IMF device may address how and why these cell types react to NT-3. Firstly, our results indicate the preferred location of neurite terminals at the end of a fixed duration of growth. It is possible that neurites never extended into the NT-3 deficient region, or that they initially proliferated within the NT-3 deficient region but then retracted before we fixed the tissue. These possibilities highlight two potential mechanisms of NT-3 directed growth: tropic (guiding neurite growth) or trophic (enhancing neurite survival). In order to examine the mechanism of NT-3 directed growth one might terminate parallel experiments at several different time points to piece together the evolution of neurite growth in the microchannel network. Secondly, our results indicate that the growth preference of both neurites and glial cells can be assessed using the IMF device. One might explore the relationship between neurite and glial preference by dissociating spiral ganglion explants and characterizing the NT-3 preference of the neurites and glial cells independently. After establishing the intrinsic preference of each cell type, one could assess the preference of the two species in co-culture in order to determine their mutual dependence. Double labeling of neurites and glial cells would help clarify their interaction during the co-culture experiments, though a more specific neurofilament antibody may be required.

In Fig. 7 we schematize four assays that could be performed using our plate with no modifications, and an additional assay requiring a change in the microfluidic network design. Our explant experiments confirm the validity of neurite growth preference assays (Fig. 7a) and the possibility of dissociated cell motility or proliferation assays (Fig. 7b).

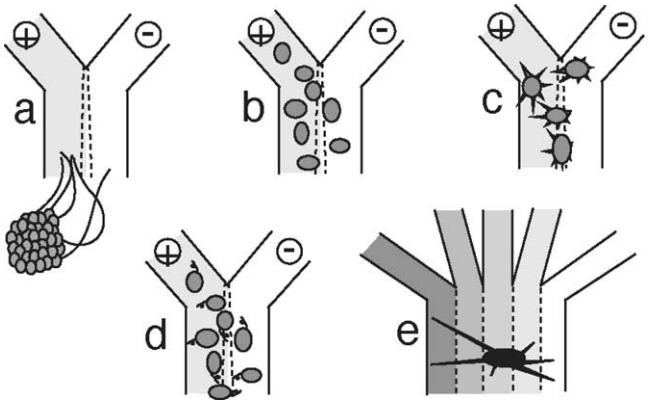

Fig. 7. Possible assays with the IMF plate. The presentation region in five different assay configurations. Shading indicates fluid with + and − solute concentrations. Dashed lines represent the boarders of the free-choice region. (a) Neural explant culture demonstrating neurites growing towards the microchannel network and preferred termination concentration. (b) Dissociated cell culture demonstrating proliferative or motile preference concentration. (c) Low density neural culture demonstrating neurite sprouting preference. (d) Motile microorganisms screen with concentration preference. (e) Modified network configuration (Dertinger et al., 2001) with low density neural culture demonstrates soluble gradient preference of extending neurites.

When making a free-choice decision, the cell or cellular process should be big enough to sample the environment on both sides of the microchannel, but small enough to clearly choose one side. With appropriately sized microchannels, cell growth preference (Fig. 7b) and neuronal process outgrowth (Fig. 7c) can be quantified using our plates. To study dissociated cells with the IMF plate, the cells should be plated onto the petri dish before compression.

The single cell preference assessment can be extended to small organisms (Fig. 7d), such as protozoa, nematodes, and paramecium, where behavioral response to differing conditions could be used to screen mutants. Mutant paramecia that are attracted to molecules in the '+' fluidic well may collect there to be harvested for further analysis later. We also suggest a modified version of our alternate-choice network which incorporates the gradient network of Dertinger et al. (2001) for neurite gradient preference assessment (Fig. 7e). In this case, the convenience of quantifying an alternate-choice is replaced by the precise control a smooth gradient of soluble growth factors. To quantify results from gradient preference assays would therefore require comparison of the number and length of extending neurites using different gradient conditions (Dertinger et al., 2002), rather than the convenience of tallying the alternate-choice binary response. Assays are not limited to growth promoting factors, but can also include assessing growth inhibitors, comparing preference between two competing stimulants, and determining isolated microenvironments for promoting survival in a partially toxic environment. A number of specific applications of the device are possible. For example, we are interested in directing dendritic innervation to the individual electrodes of an electrical cochlear implant, in order to increase its specificity in conveying information to the auditory nerve (e.g. Fu and Shannon, 1999; Wittig, 2001; Brors et al., 2002). We have quantitatively demonstrated that spiral ganglion neurites choose to grow in an NT-3 rich environment rather than the same environment without NT-3. Our results suggest that if channels delivering growth factors could be integrated into a cochlear implant, it may be possible to induce the directed growth of small groups of neurites toward specific electrodes. Similar issues of targeted innervation exist in other systems for which neural process regeneration is desirable.

Acknowledgements

This work was supported in part by grant DC00139 from the NIH/NIDCD and the Research Service of the Veterans Administration. We thank Jaakko Salonen for all fabrication guidance and suggestions. We thank Christoph Aletsee and Kwang Pak for assistance with tissue collection.

References

Aletsee C, Beros A, Mullen L, Palacios S, Pak K, Dazert S, et al. The disintegrin kistrin inhibits neurite extension from spiral ganglion explants cultured on laminin. Audiol NeuroOtol 2001a;6:57–65.

Aletsee C, Beros A, Mullen L, Palacios C, Pak K, Dazert S, et al. Ras/MEK but not p38 signaling mediates NT-3 induced neurite extension from spiral ganglion neurons. JARO 2001b;2:377–87.

Aletsee C, Brors D, Mlynski R, Ryan AF, Dazert S. Wortmannin, a specific inhibitor of phosphatidylinositol-3-kinase influences neurotrophin-induced spiral ganglion neurite growth. Larygol-Rhino-Otol 2002;81:189–95 [in German].

Aletsee C, Brors D, Mlynski R, Ryan AF, Dazert S. Branching of spiral ganglion neurites is induced by focal application of fibroblast growth factor-1. Laryngoscope 2003;113(5):791–6.

Brors D, Aletsee C, Schwager C, Mlynski R, Hansen S, Schafers M, et al. Interaction of spiral ganglion neuron processes with alloplastic materials in vitro. Hear Res 2002;167:110–21.

Brors D, Bodmer D, Pak K, Aletsee C, Schafers M, Dazert S, Ryan AF. EphA4 provides repulsive signals to developing cochlear ganglion neurites mediated through ephrin-B2 and -B3. J Comp Neurol 2003;462:90–100.

Campenot RB. Development of sympathetic neurons in compartmentalized cultures. I. Local control of neurite growth by nerve growth factor. Dev Biol 1982;93:1–12.

Chang S, Popov SV. Long-range signaling within growing neurites mediated by neurotrophin-3. Proc Natl Acad Sci 1999;96:4095–100.

Dazert S, Kin D, Luo L, Aletsee C, Garfunkel S, Maciag T, et al. Focal delivery of fibroblast growth factor-1 by transfected cells induces spiral ganglion neurite targeting in vitro. J Cell Physiol 1998;177:123–9.

Dertinger SK, Chiu DT, Jeon NL, Whitesides GM. Generation of gradients having complex shapes using microfluidic networks. Anal Chem 2001;73(6):1240.

Dertinger SK, Jiang X, Li Z, Murthy VN, Whitesides GM. Gradients of substrate-bound laminin orient axonal specification of neurons. Proc Natl Acad Sci USA 2002;99(20):12542–7 [October 1].

Duffy DC, McDonald JC, Schueller OJ, Whitesides GM. Rapid prototyping of microfluidic systems in poly(dimethylsiloxane). Anal Chem 1998;70(23):4974.

Durston AJ, Timmermans JP, Hage WJ, Hendriks HF, de Vries NJ, Heideveld M, et al. Retinoic acid causes an anteroposterior transformation in the developing central nervous system. Nature 1989;340(6229):140–4 [July 13].

Fu Q-J, Shannon RV. Effects of electrode location and spacing on speech recognition with the nucleus-22 cochlear implant. Ear Hear 1999;20(4):321–31.

Gribbon P, Hardingham TE. Macromolecular diffusion of biological polymers measured by confocal fluorescence recovery after photobleaching. Biophys J 1998;75(2):1032–9.

Hall ZW. An introduction to molecular neurobiology. Sunderland, MA: Sinauer Associates; 1992.

Hopker VH, Shewan D, Tessier-Lavigne M, Poo M, Holt C. Growth-cone attraction to netrin-1 is converted to repulsion by laminin-1. Nature 1999;401:6748–69.

Hossain WA, Brumwell CL, Morest DK. Sequential interactions of fibroblast growth factor-2, brain-derived neurotrophic factor, neurotrophin-3, and their receptors define critical periods in the development of cochlear ganglion cells. Exp Neurol 2002;175(1):138–51.

Kelley MW, Bianchi LM. Development and neuronal innervation of the organ of Corti. In: Willott JF, editor. Handbook of the mouse auditory research: from behavior to molecular biology. New York: CRC; 2001. p. 137–56.

Malgrange B, Lefebvre PP, Martin D, Staecker H, Van de Water TR, Moonen G. NT-3 has a tropic effect on process outgrowth by postnatal auditory neurones in vitro. NeuroRep 1996a;7:2495–9.

Malgrange B, Lefebvre P, Van de Water TR, Staecker H, Moonen G. Affects of neurotrophins on early auditory neurons in cell culture. NeuroRep 1996b;4:913–7.

Murray MJ, Whitington PM. Effects of roundabout on growth cone dynamics, filopodial length, and growth cone morphology at the midline and throughout the neuropile. J Neurosci 1999;19(18):7901–12 [September 15].

Negro A, Tavella A, Grandi C, Skaper SD. Production and characterization of recombinant rat brain-derived neurotrophic factor and neurotrophin-3 from insect cells. J Neurochem 1994;62:471–8.

Ono K. Free-choice preference under uncertainty. Behav Process 2000;49(1):11–9 [March 31].

Song HJ, Ming GL, Poo MM. cAMP-induced switching in turning direction of nerve growth cones. Nature 1997;388(6639):275–9.

Takayama S, McDonald JC, Ostuni E, Liang MN, Kenis PJ, Ismagilov RF, et al. Patterning cells and their environments using multiple laminar fluid flows in capillary networks. Proc Natl Acad Sci USA 1999;96(10):5545–8 [May 11].

Vozzi G, Flaim CJ, Ahluwalia A, Bianchi F, Bhatia SN. Microfabricated PLGA scaffolds: a comparative study for application to tissue engineering. Mater Sci Eng 2002;20(1–2):43–7.

Vozzi G, Flaim CJ, Ahluwalia A, Bhatia SN. Fabrication of PLGA scaffolds using soft lithography and microsyringe deposition. Biomaterials 2003;24:2533–40.

Weigl BH, Bardell RL, Kesler N, Morris CJ. Lab-on-a-chip sample preparation using laminar fluid diffusion interfaces—computational fluid dynamics model results and fluidic verification experiments. Fresenius J Anal Chem 2001;371(2):97–105 [September].

Weiss T. Cellular biophysics. Cambridge, MA: MIT Press; 1996.

Wittig Jr. J. Controlled guidance of spiral ganglion neurite growth. Masters thesis in electrical engineering at University of California, San Diego; 2001.